Nanoscale Research Letters

RESEARCH

Open Access

Scalable Moiré Lattice with Oriented TMD Monolayers

Meng-Hsi Chuang[1], Chun-An Chen[1], Po-Yen Liu[1], Xin-Quan Zhang[1], Nai-Yu Yeh[1], Hao-Jen Shih[1] and Yi-Hsien Lee[1,2*]

Abstract

Moiré lattice in artificially stacked monolayers of two-dimensional (2D) materials effectively modulates the electronic structures of materials, which is widely highlighted. Formation of the electronic Moiré superlattice promises the prospect of uniformity among different moiré cells across the lattice, enabling a new platform for novel properties, such as unconventional superconductivity, and scalable quantum emitters. Recently, epitaxial growth of the monolayer transition metal dichalcogenide (TMD) is achieved on the sapphire substrate by chemical vapor deposition (CVD) to realize scalable growth of highly-oriented monolayers. However, fabrication of the scalable Moiré lattice remains challenging due to the lack of essential manipulation of the well-aligned monolayers for clean interface quality and precise twisting angle control. Here, scalable and highly-oriented monolayers of TMD are realized on the sapphire substrates by using the customized CVD process. Controlled growth of the epitaxial monolayers is achieved by promoting the rotation of the nuclei-like domains in the initial growth stage, enabling aligned domains for further grain growth in the steady-state stage. A full coverage and distribution of the highly-oriented domains are verified by second-harmonic generation (SHG) microscopy. By developing the method for clean monolayer manipulation, hetero-stacked bilayer (epi-WS_2/epi-MoS_2) is fabricated with the specific angular alignment of the two major oriented monolayers at the edge direction of 0°/±60°. On account of the optimization for scalable Moiré lattice with a high-quality interface, the observation of interlayer exciton at low temperature illustrates the feasibility of scalable Moiré superlattice based on the oriented monolayers.

Keywords: Transition metal dichalcogenide, Scalable, Epitaxial monolayer, Moiré superlattice, Interlayer exciton

Introduction

Moiré lattice formed in the stacked monolayers of two-dimensional (2D) materials effectively modulates the electronic structures of materials, which raise considerable attentions in condensed matter physics and material sciences. Coupling among various electronic structures of the artificially stacked 2D lattices enables unique properties, such as non-conventional superconductivity [1, 2] quantized states of the interlayer exciton [3–6], and quantum emitting arrays [7] at a specific stacking and small twisting angle. With a precise twisting angle control of the hetero-stacked bilayer, the formation of Moiré superlattices promises the prospect of uniformity among different electronic moiré cells across the entire crystalline lattice. Currently, the Moiré 2D lattice has been mainly achieved by stacked bilayer of the exfoliated monolayers with a limited crystal size [8–11] or the synthesized monolayers with random orientation [12, 13], resulting in a limited size of the Moiré lattice. Fabrication of scalable Moiré lattice remains challenging due to the lack of essential manipulation of the highly-oriented monolayers. It is required to develop a clean and robust method to hetero-integrate the scalable monolayers with twisting angle control for scaling the Moiré 2D lattice [14, 15].

*Correspondence: yhlee.mse@mx.nthu.edu.tw
[1] Department of Materials Science and Engineering, National Tsing Hua University, Hsinchu 30013, Taiwan
Full list of author information is available at the end of the article

Recently, epitaxial growth of the monolayer TMD was achieved on the sapphire substrate by chemical vapor deposition (CVD) to realize scalable synthesis of the highly-oriented monolayers [16–21]. Hetero-epitaxial growth of the highly-oriented monolayer has been highlighted and widely studied for understanding of the fundamental mechanism to control the material orientation well. The well-aligned domains of the 2D materials were achievable by controlling rotation of the as-grown domains in the initial growth [22, 23] and step edges of the single crystalline substrate [24–28]. Epitaxial growth of the monolayer molybdenum disulfide (MoS_2) was optimized with the position for high S/Mo precursor concentration ratio by two-step growth at specific temperatures [19]. An additional heating stage at a lower temperature for the nucleation process promoted rotations of the grown nuclei-like domains to align the underneath single crystalline substrate for a highly-oriented film. However, more experimental studies on the growth are required for new materials and a better understanding of fundamental mechanisms. Moreover, hetero-integrating the highly-oriented monolayers for various hetero-stacked bilayers provides an opportunity to scale Moiré lattice, which is essential for exploring novel properties with the Moiré superlattice.

In this study, epitaxial growth of the highly-oriented TMDs (WS_2 and MoS_2) is achieved with a customized CVD process. A controlled growth is observed with separated growth stages at different working temperatures. A full coverage and distribution of the highly oriented domains are verified by second-harmonic generation (SHG) microscopy. A large-area Moiré lattice is fabricated by stacking the highly-oriented monolayer TMDs (epi-WS_2/ epi-MoS_2) with a small twisting angle and a clean manipulation method. Photoluminescence (PL) measurement of the scalable Moiré is carried out at a low temperature of 77 K to verify the interlayer exciton and interface quality of the hetero-stacked bilayer.

Methods/Experimental

The Growth of Epitaxial Monolayer Tungsten Disulfide (WS_2)

Epitaxial monolayer WS_2 was synthesized on the sapphire substrate by the ambient-pressure chemical vapor deposition (APCVD). Solid precursors, including WO_3 (600 mg, Alfa Aesar, 99.8% CAS# 1314-35-8) and Sulfur (10 mg, Sigma-Aldrich 99.5% CAS#7704-34-9) powders, were used for the CVD synthesis. The as-grown sapphire substrates were placed face-down on the WO_3 crucible in the middle of furnace and S crucible was located on the upstream within the heating belt. The furnace was heated to the growth temperature of 950 °C. A gas flow of the mixed H_2/Ar was 2/20 sccm in the initial growth stage and then 5/120 sccm in the steady state stage. After keeping for 5 min, the furnace was shut down and natural cooling.

The Growth of Epitaxial Monolayer Molybdenum Disulfide (MoS_2)

Epitaxial monolayer MoS_2 was synthesized on the sapphire substrate by the low-pressure CVD (LPCVD). The growth condition was under ~ 5 torr with a temperature range from 750 to 900 °C. Solid precursors, including MoO_3 (50 mg, Alfa Aesar, 99.5% CAS#1313-27-5) and Sulfur (500 mg, Sigma-Aldrich 99.5% CAS#7704-34-9) powders, were used for the CVD synthesis. The as-grown sapphire substrates were placed face-up in the middle of furnace at the downstream of the sequential S and Mo crucibles. Ar gas flow ~ 200 sccm was blown for an inert atmosphere. The furnace was heated to achieve a temperature of 800 °C, for a relatively low nucleation and then further heated to achieve the growth temperature of 950 °C. Relative to multi-stage heating process for Mo powders, the sulfur was directly heated to 250 °C in the beginning of the experiment to maintain the sufficiency of sulfur precursors concentration. After keeping for 5 min, the furnace was shut down and naturally cooled.

PDMS Stamping for Clean Manipulation

The PDMS stamps were prepared using the mixed pre-polymer and cross-linker at a weight ratio of 10:1 with a curing time of 48 h at room temperature under vacuum situation. During the transfer, the PDMS stamp was first placed on an as-grown monolayer. After submerged into deionized water, the PDMS was carefully lifted and placed TMDs side up on a quartz slide. The quartz slide was then being fixed under the optical microscope with a XYZ rotatable stage beneath. The target sample was brought in contact with the PDMS stamp by the stage at the desirable position and twisting angular degree, resulting in a stacking hetero-stacked bilayer. Finally, the stacked sample was heated to 70 °C, causing the PDMS to lose its stickiness before removed.

Material Analysis

Optical microscopy (OM) and Atomic force microscopy (AFM) are used to characterize the surface morphology and microscale structure for epi-TMD films. The highly-oriented domains and their morphologies are observed by the optical microscopy (Olympus-BX51). We could distinguish the monolayer TMD by a clear contract and verify the various of thickness with the color of different shades for the initial judgment. Scanning Probe Microscopy is performed by Bruker Dimension® Icon with basic tapping mode height profile measurement by TESPA tips.

SHG Nonlinear Microscopy

A customized nonlinear microscope, based on Leica SP5 confocal microscope is operated in non-descan mode and equipped with motorized tuning capabilities in in-plane directions (x, y) and azimuthal rotation (ϕ). The wavelength of fundamental wave (FW) laser is set to 810 nm for the whole SHG measurement and focused on the sample with a $10\times$ objective lens. Through this setup, SHG mapping over large-area region could be efficiently obtained. While rotating the sample, which is fixed on the stage, angle (φ_{FW-D}) between the polarization of incident FW laser and the armchair direction of the monolayer TMD domain can be adjusted.

Raman and PL Microscopy

Raman and micro-PL spectroscopy are utilized with a confocal microscope system, equipped with a 532 nm continuous wave (CW) pumping laser at room temperature. (Micro Raman/PL/TR-PL Spectrometer, Ramaker, Protrustech). $50\times$ Long working distance objective lens are used with a spot size of the laser around 1–2 μm for full-range temperature experiment from 77 K to room temperature. Temperature Control Systems for Microscopy and Spectroscopy are carried out to measure the optical properties under low temperature (THMS350V, Linkam Scientific). Typical gratings are used with 300 g/mm for PL (low resolution) to get broadband spectrum and 1800 g/mm for Raman (high resolution) signals to get the detail information of material.

Results and Discussion

Van der Waals (vdW) epitaxy was achieved for the highly-oriented TMD monolayer by controlling surface structures of the single crystalline sapphire substrate with a reduced formation energy under certain surface termination [29–31] and small lattice mismatch [17, 18]. With our customized CVD process, the monolayer TMDs (MoS_2 and WS_2) are epitaxially grown on the sapphire with two major orientations ($0°/\pm 60°$ to the edge). The growth of highly-oriented TMDs is achieved and optimized by controlling growth conditions in the two representative growth periods, as shown in Fig. 1a, b, respectively. Two stages including nuclei-like domain rotating in the initial growing stage and grain size extending in the steady state stage dominate the synthesized process and the schematics of the growth mechanism are demonstrated. In the initial growth stage, some misoriented nuclei-like domains are observed and rotatable with reaction of small amounts of precursors at a relatively lower temperature. In Fig. 1a, the rotation only appears at a low temperature of 800–850 °C with a smaller domain size, leading to a pair of orientations for the lowest energy states. With the increase in working temperature, the growth behavior prefers lateral growth than formation of more nuclei-like domains by suitable control of reacting conditions. In the steady state growth stage, lateral growth of the aligned domains appears and forms a full coverage of highly-oriented monolayer TMD at a high temperature of 950 °C, as shown in Fig. 1b. With the optimized conditions, the aligned domains become

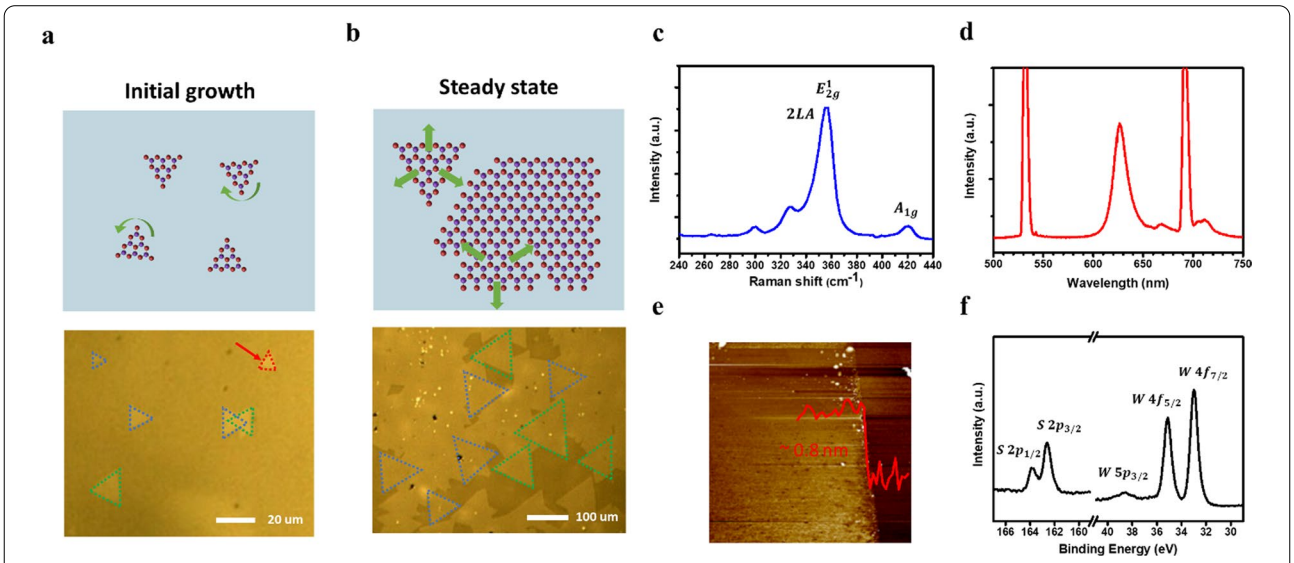

Fig. 1 The scalable epitaxial growth of highly-oriented monolayer TMDs by customized CVD process. Schematics illustration of growth mechanism in the **a** initial growing stage and **b** steady state stage with related OM images. **c** Raman, **d** PL, **e** height profile and **f** XPS analysis of epitaxial monolayer WS_2

non-rotatable in the stage of steady-state growth, enabling the vdW epitaxy for the synthesized monolayer TMD with aligned domains at a pair of the preferred orientations at 0° and ± 60°.

To obtain more highly-oriented monolayer TMDs for scalable Moiré lattice of the stacked bilayer, monolayer of highly-oriented MoS_2 was epitaxially grown on the sapphire substrate, which was consistent to the reported work [19]. To enable vdW epitaxy of the MoS_2 for highly-oriented monolayer, a setup of low-pressure CVD is effective for optimizing the growth in the sufficiency of sulfur vapor concentration (detailed information is described in the "method/experimental" section). Additional file 1: Figure S1 demonstrates the statistical analysis for the aligned domains (at 0° and ± 60°) of the large-area monolayer MoS_2 epitaxially grown on sapphire substrates. Transitions from randomly-oriented to well-aligned domains were realized by promoting the rotation for aligned domains in the initial growth and sequentially growing in the second growth stage at a higher growth temperature. In contrast, epi-WS_2 film was rarely synthesized before due to the low WO_3 vaporizing pressure and bad reactivity. Large-area monolayer WS_2 film was epitaxially grown on sapphire substrates by using ambient-pressure CVD with a heating belt system, as shown the schematic illustration in Additional file 1: Figure S2a). Reduced concentration of the precursors and a high ratio (S/W) of the chalcogen to transition metals, achieved with an increased Ar gas flow in the steady state stage and a controlled sulfur vapor in the initial growth stage, significantly promoted the vdW growth for the highly-oriented monolayer TMD. Additional file 1: Figure S2b–e presents the influence of H_2 flow on the lateral growth of highly-oriented monolayer WS_2 to grow the epitaxial film. Similar to the growth of the MoS_2, synthesis of the highly-oriented WS_2 was optimized by controlling growth parameters for enhanced nucleation and growth of the monolayer with a larger domain size and higher quality.

In Fig. 1b, optical microscope (OM) image of the large-area and highly-oriented monolayer WS_2 indicated that the aligned domains were over 90% coverage with an average size of 100–200 μm. Figure 1c shows the characteristic Raman spectrum where the vibration mode of 2LA(M), E_{2g}, and A_{1g} peak are located at 351 cm^{-1}, 355 cm^{-1}, and 417 cm^{-1}, respectively, suggesting the high-quality monolayer crystal structure. Photoluminescence (PL) spectrum with the peak position of 626 nm exhibited the optical property of the direct band gap structure, as shown in Fig. 1d. In addition, the thickness of monolayer epi-WS_2 was verified ~ 0.8 nm with the atomic force microscopy (AFM) as presented in Fig. 1e. Figure 1f shows the binding energy of S 2*p* and W 4*f* core level for the X-ray photoelectron spectroscopy (XPS) analysis and no obviously additional peaks exhibit that the material was relatively uniform without damage and oxidation.

Distribution on the orientation of the single crystalline domains in the TMD materials determines the symmetry of artificially stacked bilayer, which is significant to entire band structures and nonlinear optical properties [32–34]. Second harmonic generation (SHG) microscopy is adopted to further verify the spatial variations of the orientation in the scalable and highly-oriented monolayer TMDs. The 2H phase of the monolayer TMD (MoS_2 and WS_2) exhibits $D_{3h}{}^1$ symmetry group with a broken inversion symmetry, which enables a high second-order nonlinear optical susceptibility [35, 36]. While rotating the sample, angular degree (φ_{FW-D}) between the polarization of incident FW laser (black arrow) and the armchair direction of the TMD domain (blue arrow) can be adjusted as shown in Fig. 2a. The emitting SHG intensity shows an angular dependence of $\cos^2(3\varphi_{FW-D})$ with respect to the FW laser polarization (Fig. 2b). The brightness evolution, shown in Fig. 2c, is in good agreement with the measured polarization-resolved SHG emission. With the mapping of the SHG intensity, the single crystalline domain exhibits the same intensity at the edge orientation of 0° and ± 60°, while grains with other orientation angles can be easily distinguished because of the darker emissions. Such polarization-sensitive optical nonlinearity is powerful on the determination of the twisting angle. Figure 2d and Additional file 1: Figure S3 show the SHG intensity map with scaled color contour between an epitaxial and a non-epitaxial film. Statistical analysis from intensity map exhibited that the preferred orientation for the as-grown epi-MoS_2 increased from 80% with half coverage up to over 95% with full coverage. The result motivates further efforts to focus on the development of Moiré hetero-stacked bilayer with coherently stacking.

The large-area Moiré superlattice was stacked by transferring the scalable highly-oriented WS_2 on the as-grown scalable highly-oriented MoS_2 with the polydimethylsiloxane (PDMS) assisted water transfer technique [37–40] for interfacial cleanness and precise twisting angle control. A transparent, flat and flexible PDMS film was adopted as a supporting layer and the stacking sample (PDMS/epi-TMD film) was gently lifted-off from the as-grown substrates after immersing into the deionized water. The PDMS/material film was then fixed on the quartz slide under the XYZ rotatable stages system, and precisely stamped on the highly-oriented heterostructure at the target substrate with a desirable position and twisting angle, resulting in an angle-controlled hetero-stacked bilayer. Finally, the stacked sample was heated

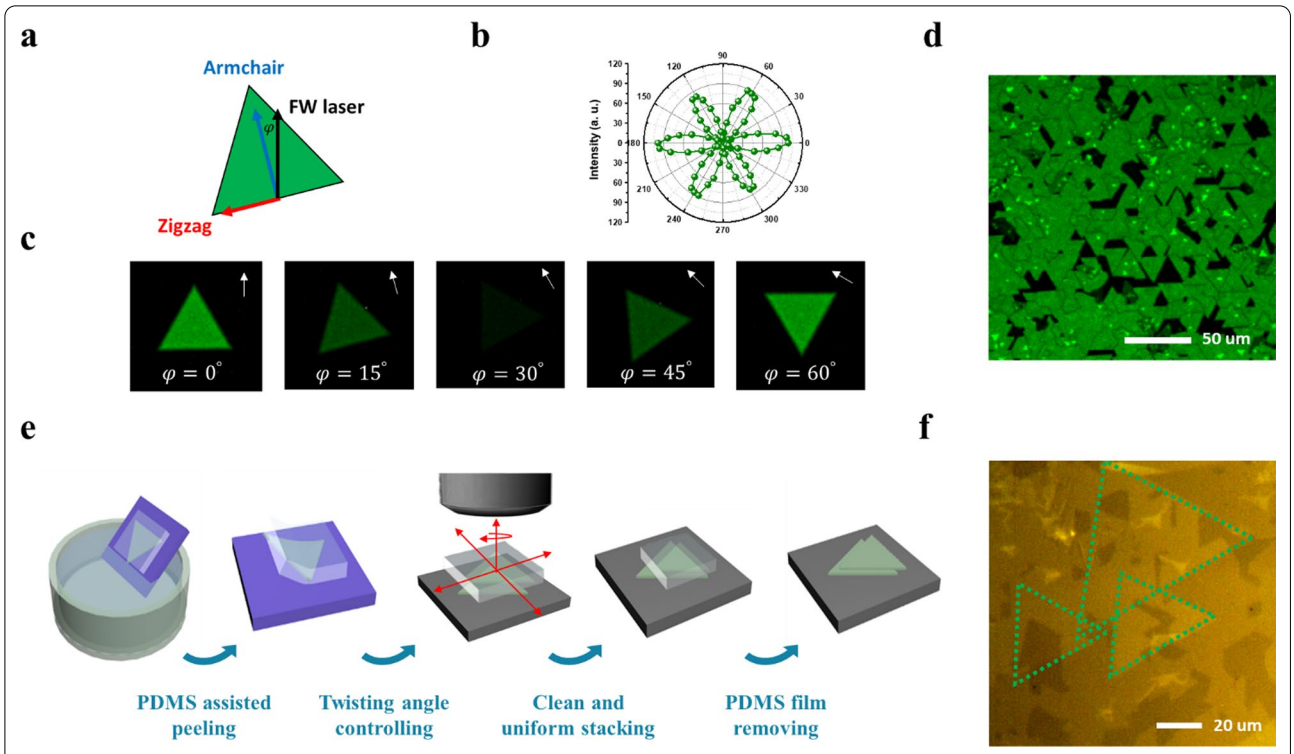

Fig. 2 Integrating the oriented TMD for scalable Moiré lattice with twisting control. **a** Schematic illustration of TMD with zigzag and armchair direction, while φ is defined as the angle between the polarization of incident FW laser and the armchair direction of the TMD. **b** Polar plot of polarization resolved SHG intensity. **c,** The SHG mapping images for monolayer MoS_2 grain with misaligned angles (φ_{FW-D}) between 0° and 60°. **d** The SHG intensity mapping of epi-TMD film. **e** Schematics illustration of clean water transfer technique with PDMS stamping. **f** OM images of the stacked hetero-bilayer

to 70 °C and the PDMS thin film without stickiness was peeled off with clean surface. The schematic transfer process is illustrated in Fig. 2e and more detail is shown in the "method/experimental" section. Since the bottom layer of highly-oriented monolayer TMD stays atomically flat on the as-grown substrate and the sequential transferred monolayer epi-TMD is stacked on top of that by clean water transferring, the large-area hetero-stacked bilayer would be achieved with a high interfacial quality and ultra-clean surface. Figure 2f shows the OM image of a hetero-stacked bilayer for epi-WS_2/epi-MoS_2. The optical image demonstrated the uniformity and cleanness throughout the stacked epitaxial monolayers. Furthermore, the precision of the bilayer twist angle could be assured from the sharp edges of the two TMD materials.

To study optical properties of the hetero-stacked bilayer, Raman and micro-PL spectroscopy were obtained with a confocal microscope system. Figure 3d shows the Raman spectra of the highly-oriented monolayer TMDs (MoS_2 and WS_2) which are compared with that of the stacked WS_2/MoS_2 heterostructures (Fig. 3a) on the sapphire substrate. Two Raman vibration peaks were revealed at 383 and 404 cm^{-1}, corresponding to the in-plane E_{2g} and out of plane A_{1g} vibrational modes of MoS_2, while the main feature peaks located at 351, 355, and 417 cm^{-1}, corresponding to second-order mode of longitudinal acoustic phonon 2LA(M), in-plane E_{2g}, and out-of-plane A_{1g} of WS_2, respectively. The Raman spectra measured in the heterostructure bilayer contained both the characteristic peaks of MoS_2 and WS_2. Furthermore, we observed that the peak position of the Raman A_{1g} modes stiffened about 2–3 cm^{-1} in the stacked samples attributed to strong interlayer coupling, which was consistent with previous papers [39, 41, 42]. Figure 3e similarly collects the PL signals from epi-films of MoS_2, WS_2, and the hetero-bilayer area at room temperature, respectively. Strong photoemission displayed at 667 nm (~ 1.83 eV), which corresponds to the A excitonic transitions for MoS_2, while two peaks located at 615 nm and 626 nm, which corresponds to the exciton and trion emission for WS_2. The PL spectra measured at room temperature in the heterojunction region exhibited the obvious PL quenching phenomenon compared to the dual monolayer region, also indicating the cleanness of WS_2 /MoS_2 interface with strong interlayer coupling [41, 43, 44].

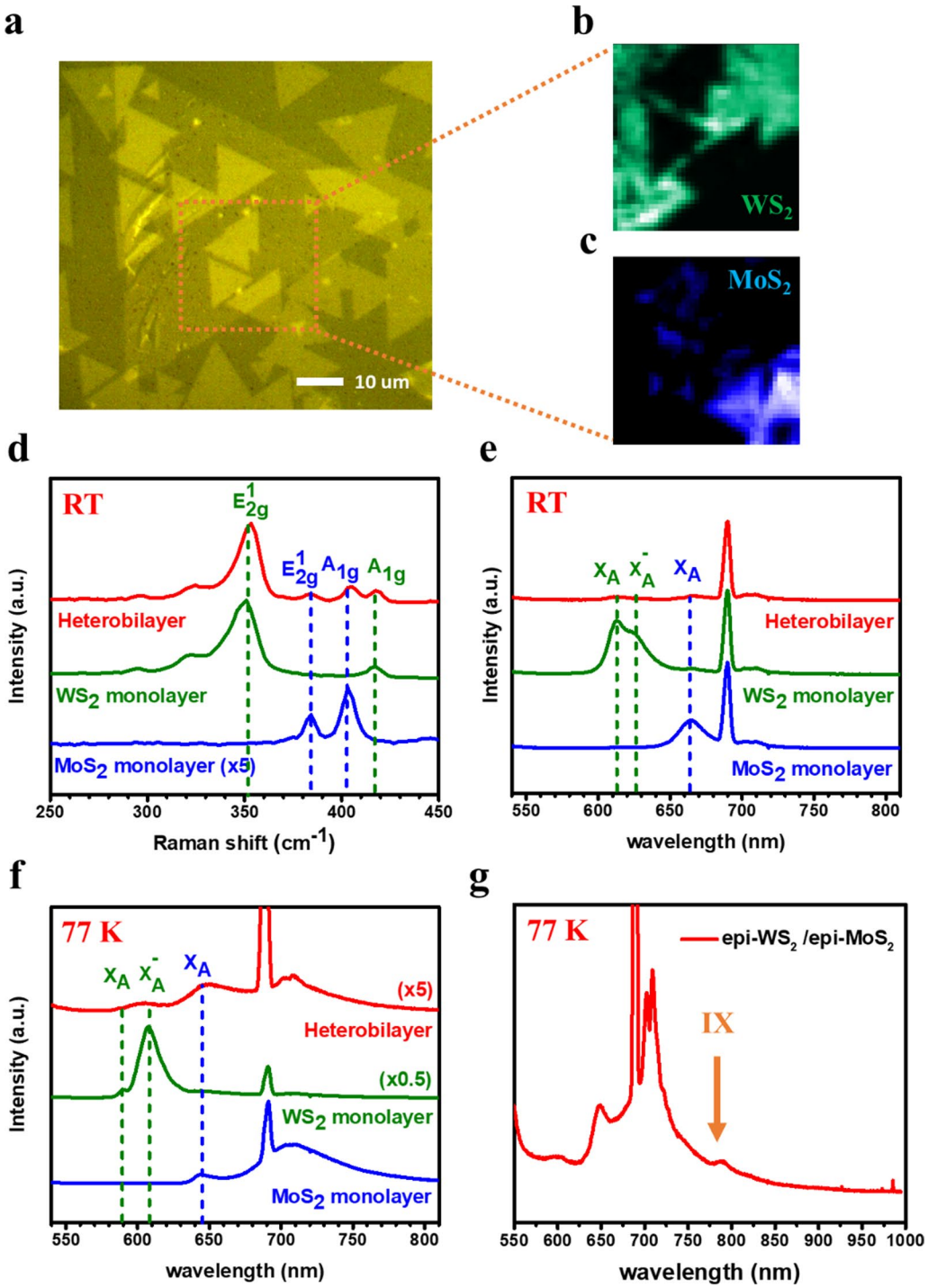

Fig. 3 Strong interlayer coupling at the stacked bilayer of the oriented monolayers. **a** OM image of the stacked bilayer of the epi-WS_2 and the epi-MoS_2. PL mapping of **b** epitaxial monolayer WS_2 and **c** epitaxial monolayer MoS_2. **d** Raman and **e** PL spectra at room temperature. **f** PL spectra and **g** interlayer exciton emission at low temperature of 77 K

The low-temperature PL characterization at 77 K was performed to further identify the interface quality and performances of the scalable Moiré lattice. Both oriented monolayers of the WS_2 and the MoS_2 exhibited an obvious blue-shift of PL peaks, as shown in Fig. 3f. The A-exciton emission position of the MoS_2 shifted from

667 to 646 nm, which can be attributed to the change in lattice size with the decrease in temperature. The spectral weight of WS_2 shifted from exciton (590 nm) to trion (609 nm) indicating that the thermal energy at higher temperature is large enough to lead to a partial dissociation of the trions [45]. In the spectrum of the MoS_2, a broaden peak at ~ 710 nm represents the defect peak of the epi-MoS_2. The low temperature intensity mappings of MoS_2 PL characteristic peak at 646 nm, and WS_2 trion peak at 609 nm were shown, respectively, in Fig. 3b, c, corresponding to the field of view of the white rectangular region in Fig. 3a. The obvious quenching of both characteristic peaks was observed from the intensity map as the same interlayer effect at the room temperature. The magnified PL spectrum of the hetero-bilayer region, presented in Fig. 3f contained both the characteristic peaks, corresponding to direct excitonic transition energies in monolayer MoS_2 and WS_2 while the substrate peaks were located around 700 nm. Moreover, there was a weak peak at ~ 790 nm (~ 1.57 eV) which could be represented by the interlayer exciton emission (Fig. 3g). It is noteworthy that the evidence of interlayer exciton is visualized without the h-BN capping, suggesting a high quality of the hetero-interface. Inhomogeneity on interlayer interactions is due to variation of the hetero-interface at stacked monolayer. In future studies, scalable integration of the synthesized h-BN with the Moiré lattice would effectively improve the homogeneity of the interlayer interactions. These above observations confirm an ideal interface between the scalable and highly-oriented monolayer (WS_2 and MoS_2) for strong interlayer coupling of physical parameters, which move a significant step toward large-area Moiré heterostructure.

Conclusions

Scalable highly-oriented monolayer TMDs (WS_2 and MoS_2) are hetero-epitaxially grown with customized CVD by controlling working temperature of growth stages. Controlled growth is achieved by promoting rotation of the nuclei-like domains with the growth parameters to well align the single crystalline substrates in the initial growth and growth of domains to the unidirectional film in the steady state. Coverage and distribution of the highly-oriented domains are verified by SHG microscopy. With the PDMS-assisted transfer method for a clean manipulation, large-area hetero-stacked bilayer of the two oriented monolayers (epi-WS_2/epi-MoS_2) is fabricated with a twisting angle control. The interlayer exciton observed at 77 K confirms the interface quality and uniformity of the Moiré lattice. Scalable Moiré lattices move a significant step toward artificial electronic structures of 2D lattices.

Abbreviations

2D: Two-dimensional; TMD: Transition metal dichalcogenide; CVD: Chemical vapor deposition; OM: Optical microscope; AFM: Atomic force microscopy; PL: Photoluminescence; XPS: X-ray photoelectron spectroscopy; SHG: Second harmonic generation.

Supplementary Information

The online version contains supplementary material available at https://doi.org/10.1186/s11671-022-03670-y.

Additional file 1. Scalable synthesis of epitaxial monolayer TMDs.

Authors' Contributions

MHC, and YHL co-wrote the paper. MHC, XQZ, NYY, and HJS performed the epitaxial growth of monolayer TMDs. CAC, and PYL fabricated the transferred hetero-bilayer and measured the related optical properties. YHL designed and supervised the project. All authors discussed the results and commented on the manuscript at all stages. All authors read and approved the final manuscript.

Funding

We acknowledge support from AOARD grant (co-funded with ONRG) FA2386-16-1-4009, Ministry of Science and Technology (MOST 109-2124-M-007 -001 -MY3, MOST 108-2112-M-007-006-MY3, MOST 107-2923-M-007-002-MY3, MOST 106-2119-M-007-023-MY3, and MOST 105-2112-M-007-032-MY3), and Academia Sinica Research Program on Nanoscience and Nanotechnology (AS-iMATE-107-11and AS-iMATE-109-11). This work was partially supported by the "Frontier Research Center on Fundamental and Applied Sciences of Matters" and "Center for Quantum Technology" of National Tsing Hua University from The Featured Areas Research Center Program within the framework of the Higher Education Sprout Project by the Ministry of Education (MOE) in Taiwan.

Availability of Data and Materials

All data generated during this study are included in this published article and its supplementary information files.

Declarations

Competing interests

The authors declare that there are no competing interests.

Author details

[1]Department of Materials Science and Engineering, National Tsing Hua University, Hsinchu 30013, Taiwan. [2]Frontier Research Center on Fundamental and Applied Sciences of Matters, National Tsing Hua University, Hsinchu 30013, Taiwan.

Received: 28 December 2021 Accepted: 30 January 2022
Published online: 14 March 2022

References

1. Cao Y, Fatemi V, Fang S, Watanabe K, Taniguchi T, Kaxiras E, Jarillo-Herrero P (2018) Unconventional superconductivity in magic-angle graphene superlattices. Nature 556(7699):43–50
2. Cao Y, Fatemi V, Demir A, Fang S, Tomarken SL, Luo JY, Sanchez-Yamagishi JD, Watanabe K, Taniguchi T, Kaxiras E, Ashoori RC, Jarillo-Herrero P (2018) Correlated insulator behaviour at half-filling in magic-angle graphene superlattices. Nature 556(7699):80–84
3. Wu F, Lovorn T, MacDonald AH (2017) Topological exciton bands in Moire heterojunctions. Phys Rev Lett 118(14):147401
4. Wu FC, Lovorn T, MacDonald AH (2018) Theory of optical absorption by interlayer excitons in transition metal dichalcogenide heterobilayers. Phys Rev B 97(3):035306
5. Baek H, Brotons-Gisbert M, Campbell A, Vitale V, Lischner J, Watanabe K, Taniguchi T, Gerardot BD (2021) Optical read-out of Coulomb staircases

in a Moire superlattice via trapped interlayer trions. Nat Nanotechnol 16(11):1237–1243
6. Yu H, Liu GB, Tang J, Xu X, Yao W (2017) Moire excitons: from programmable quantum emitter arrays to spin-orbit-coupled artificial lattices. Sci Adv 3(11):e1701696
7. Zhang L, Wu F, Hou S, Zhang Z, Chou YH, Watanabe K, Taniguchi T, Forrest SR, Deng H (2021) Van der Waals heterostructure polaritons with moire-induced nonlinearity. Nature 591(7848):61–65
8. Shabani S, Halbertal D, Wu WJ, Chen MX, Liu S, Hone J, Yao W, Basov DN, Zhu XY, Pasupathy AN (2021) Deep moire potentials in twisted transition metal dichalcogenide bilayers. Nat Phys 17(6):720–725
9. Andersen TI, Scuri G, Sushko A, De Greve K, Sung J, Zhou Y, Wild DS, Gelly RJ, Heo H, Berube D, Joe AY, Jauregui LA, Watanabe K, Taniguchi T, Kim P, Park H, Lukin MD (2021) Excitons in a reconstructed moire potential in twisted WSe_2/WSe_2 homobilayers. Nat Mater 20(4):480–487
10. Quan J, Linhart L, Lin ML, Lee D, Zhu J, Wang CY, Hsu WT, Choi J, Embley J, Young C, Taniguchi T, Watanabe K, Shih CK, Lai K, MacDonald AH, Tan PH, Libisch F, Li X (2021) Phonon renormalization in reconstructed MoS_2 moire superlattices. Nat Mater 20(8):1100–1105
11. Tang Y, Gu J, Liu S, Watanabe K, Taniguchi T, Hone J, Mak KF, Shan J (2021) Tuning layer-hybridized moire excitons by the quantum-confined Stark effect. Nat Nanotechnol 16(1):52–57
12. Wang K, Huang B, Tian M, Ceballos F, Lin MW, Mahjouri-Samani M, Boulesbaa A, Puretzky AA, Rouleau CM, Yoon M, Zhao H, Xiao K, Duscher G, Geohegan DB (2016) Interlayer coupling in twisted WSe_2/WS_2 bilayer heterostructures revealed by optical spectroscopy. ACS Nano 10(7):6612–6622
13. Susarla S, Sassi LM, Zobelli A, Woo SY, Tizei LHG, Stephan O, Ajayan PM (2021) Mapping Modified electronic levels in the Moire patterns in MoS_2/WSe_2 using low-loss EELS. Nano Lett 21(9):4071–4077
14. Chen PY, Zhang XQ, Lai YY, Lin EC, Chen CA, Guan SY, Chen JJ, Yang ZH, Tseng YW, Gwo S, Chang CS, Chen LJ, Lee YH (2019) Tunable Moire superlattice of artificially twisted monolayers. Adv Mater 31(37):e1901077
15. Choi J, Hsu WT, Lu LS, Sun L, Cheng HY, Lee MH, Quan J, Tran K, Wang CY, Staab M, Jones K, Taniguchi T, Watanabe K, Chu MW, Gwo S, Kim S, Shih CK, Li X, Chang WH (2020) Moire potential impedes interlayer exciton diffusion in van der Waals heterostructures. Sci Adv 6(39):eaba8866
16. Chen L, Liu B, Ge M, Ma Y, Abbas AN, Zhou C (2015) Step-edge-guided nucleation and growth of aligned WSe_2 on sapphire via a layer-over-layer growth mode. ACS Nano 9(8):8368–8375
17. Ji Q, Kan M, Zhang Y, Guo Y, Ma D, Shi J, Sun Q, Chen Q, Zhang Y, Liu Z (2015) Unravelling orientation distribution and merging behavior of monolayer MoS_2 domains on sapphire. Nano Lett 15(1):198–205
18. Dumcenco D, Ovchinnikov D, Marinov K, Lazic P, Gibertini M, Marzari N, Lopez Sanchez O, Kung YC, Krasnozhon D, Chen MW, Bertolazzi S, Gillet P, Fontcuberta I, Morral A, Radenovic A, Kis A (2015) Large-area epitaxial monolayer MoS_2. ACS Nano 9(4):4611–4620
19. Aljarb A, Cao Z, Tang HL, Huang JK, Li M, Hu W, Cavallo L, Li LJ (2017) Substrate lattice-guided seed formation controls the orientation of 2D transition-metal dichalcogenides. ACS Nano 11(9):9215–9222
20. Ma Z, Wang S, Deng Q, Hou Z, Zhou X, Li X, Cui F, Si H, Zhai T, Xu H (2020) Epitaxial growth of rectangle shape MoS_2 with highly aligned orientation on twofold symmetry a-plane sapphire. Small 16(16):e2000596
21. Li T, Guo W, Ma L, Li W, Yu Z, Han Z, Gao S, Liu L, Fan D, Wang Z, Yang Y, Lin W, Luo Z, Chen X, Dai N, Tu X, Pan D, Yao Y, Wang P, Nie Y, Wang J, Shi Y, Wang X (2021) Epitaxial growth of wafer-scale molybdenum disulfide semiconductor single crystals on sapphire. Nat Nanotechnol 16(11):1201–1207
22. Zhang X, Choudhury TH, Chubarov M, Xiang Y, Jariwala B, Zhang F, Alem N, Wang GC, Robinson JA, Redwing JM (2018) Diffusion-controlled epitaxy of large area coalesced WSe_2 monolayers on sapphire. Nano Lett 18(2):1049–1056
23. Chubarov M, Choudhury TH, Hickey DR, Bachu S, Zhang T, Sebastian A, Bansal A, Zhu H, Trainor N, Das S, Terrones M, Alem N, Redwing JM (2021) Wafer-scale epitaxial growth of unidirectional WS_2 monolayers on sapphire. ACS Nano 15(2):2532–2541
24. Wang J, Xu X, Cheng T, Gu L, Qiao R, Liang Z, Ding D, Hong H, Zheng P, Zhang Z, Zhang Z, Zhang S, Cui G, Chang C, Huang C, Qi J, Liang J, Liu C, Zuo Y, Xue G, Fang X, Tian J, Wu M, Guo Y, Yao Z, Jiao Q, Liu L, Gao P, Li Q, Yang R, Zhang G, Tang Z, Yu D, Wang E, Lu J, Zhao Y, Wu S, Ding F, Liu K (2021) Dual-coupling-guided epitaxial growth of wafer-scale single-crystal WS_2 monolayer on vicinal a-plane sapphire. Nat Nanotechnol. https://doi.org/10.1038/s41565-021-01004-0
25. Lu CI, Butler CJ, Huang JK, Hsing CR, Yang HH, Chu YH, Luo CH, Sun YC, Hsu SH, Yang KHO, Wei CM, Li LJ, Lin MT (2015) Graphite edge controlled registration of monolayer MoS_2 crystal orientation. Appl Phys Lett 106(18):181904
26. Yang P, Zhang S, Pan S, Tang B, Liang Y, Zhao X, Zhang Z, Shi J, Huan Y, Shi Y, Pennycook SJ, Ren Z, Zhang G, Chen Q, Zou X, Liu Z, Zhang Y (2020) Epitaxial growth of centimeter-scale single-crystal MoS_2 monolayer on Au(111). ACS Nano 14(4):5036–5045
27. Chen TA, Chuu CP, Tseng CC, Wen CK, Wong HP, Pan S, Li R, Chao TA, Chueh WC, Zhang Y, Fu Q, Yakobson BI, Chang WH, Li LJ (2020) Wafer-scale single-crystal hexagonal boron nitride monolayers on Cu (111). Nature 579(7798):219–223
28. Choi SH, Kim HJ, Song B, Kim YI, Han G, Nguyen HTT, Ko H, Boandoh S, Choi JH, Oh CS, Cho HJ, Jin JW, Won YS, Lee BH, Yun SJ, Shin BG, Jeong HY, Kim YM, Han YK, Lee YH, Kim SM, Kim KK (2021) Epitaxial single-crystal growth of transition metal dichalcogenide monolayers via the atomic sawtooth Au surface. Adv Mater 33(15):e2006601
29. Lai YY, Chuang CH, Yeh YW, Hou CH, Hsu SC, Chou Y, Chou YC, Kuo HC, Wu YS, Cheng YJ (2021) Substrate lattice-guided MoS_2 crystal growth: implications for van der Waals epitaxy. ACS Appl Nano Mater 4(5):4930–4938
30. Suenaga K, Ji HG, Lin YC, Vincent T, Maruyama M, Aji AS, Shiratsuchi Y, Ding D, Kawahara K, Okada S, Panchal V, Kazakova O, Hibino H, Suenaga K, Ago H (2018) Surface-mediated aligned growth of monolayer MoS_2 and in-plane heterostructures with graphene on sapphire. ACS Nano 12(10):10032–10044
31. Ji HG, Lin YC, Nagashio K, Maruyama M, Solis-Fernandez P, Aji AS, Panchal V, Okada S, Suenaga K, Ago H (2018) Hydrogen-assisted epitaxial growth of monolayer tungsten disulfide and seamless grain stitching. Chem Mater 30(2):403–411
32. Kumar N, Najmaei S, Cui QN, Ceballos F, Ajayan PM, Lou J, Zhao H (2013) Second harmonic microscopy of monolayer MoS_2. Phys Rev B 87(16):161403
33. Malard LM, Alencar TV, Barboza APM, Mak KF, de Paula AM (2013) Observation of intense second harmonic generation from MoS_2 atomic crystals. Phys Rev B 87(20):201401(R)
34. Jiang T, Liu H, Huang D, Zhang S, Li Y, Gong X, Shen YR, Liu WT, Wu S (2014) Valley and band structure engineering of folded MoS_2 bilayers. Nat Nanotechnol 9(10):825–829
35. Li Y, Rao Y, Mak KF, You Y, Wang S, Dean CR, Heinz TF (2013) Probing symmetry properties of few-layer MoS_2 and h-BN by optical second-harmonic generation. Nano Lett 13(7):3329–3333
36. Hsu WT, Zhao ZA, Li LJ, Chen CH, Chiu MH, Chang PS, Chou YC, Chang WH (2014) Second harmonic generation from artificially stacked transition metal dichalcogenide twisted bilayers. ACS Nano 8(3):2951–2958
37. Liu K, Yan Q, Chen M, Fan W, Sun Y, Suh J, Fu D, Lee S, Zhou J, Tongay S, Ji J, Neaton JB, Wu J (2014) Elastic properties of chemical-vapor-deposited monolayer MoS_2, WS_2, and their bilayer heterostructures. Nano Lett 14(9):5097–5103
38. Jia H, Yang R, Nguyen AE, Alvillar SN, Empante T, Bartels L, Feng PX (2016) Large-scale arrays of single- and few-layer MoS_2 nanomechanical resonators. Nanoscale 8(20):10677–10685
39. Tongay S, Fan W, Kang J, Park J, Koldemir U, Suh J, Narang DS, Liu K, Ji J, Li J, Sinclair R, Wu J (2014) Tuning interlayer coupling in large-area heterostructures with CVD-grown MoS_2 and WS_2 monolayers. Nano Lett 14(6):3185–3190
40. Niehues I, Blob A, Stiehm T, Schmidt R, Jadrisko V, Radatovic B, Capeta D, Kralj M, de Vasconcellos SM, Bratschitsch R (2018) Strain transfer across grain boundaries in MoS_2 monolayers grown by chemical vapor deposition. 2D Mater 5(3):031003
41. Zhang J, Wang J, Chen P, Sun Y, Wu S, Jia Z, Lu X, Yu H, Chen W, Zhu J, Xie G, Yang R, Shi D, Xu X, Xiang J, Liu K, Zhang G (2016) Observation of strong interlayer coupling in MoS_2/WS_2 heterostructures. Adv Mater 28(10):1950–1956
42. Susarla S, Manimunda P, Morais Jaques Y, Hachtel JA, Idrobo JC, Syed Amnulla SA, Galvao DS, Tiwary CS, Ajayan PM (2018) Deformation mechanisms of vertically stacked WS_2/MoS_2 heterostructures: the role of interfaces. ACS Nano 12(4):4036–4044

43. Hong X, Kim J, Shi SF, Zhang Y, Jin C, Sun Y, Tongay S, Wu J, Zhang Y, Wang F (2014) Ultrafast charge transfer in atomically thin MoS_2/WS_2 heterostructures. Nat Nanotechnol 9(9):682–686
44. Okada M, Kutana A, Kureishi Y, Kobayashi Y, Saito Y, Saito T, Watanabe K, Taniguchi T, Gupta S, Miyata Y, Yakobson BI, Shinohara H, Kitaura R (2018) Direct and indirect interlayer excitons in a van der Waals heterostructure of hBN/WS_2/MoS_2/hBN. ACS Nano 12(3):2498–2505
45. Plechinger G, Nagler P, Kraus J, Paradiso N, Strunk C, Schüller C, Korn T (2015) Identification of excitons, trions and biexcitons in single-layer WS2. Phys Status Solidi (RRL)–Rapid Res Lett 9(8):457–461

Publisher's Note